J|A|C|S
ARTICLES
Published on Web 02/03/2004

An EPR, ESEEM, Structural NMR, and DFT Study of a Synthetic Model for the Covalently Ring-Linked Tyrosine-Histidine Structure in the Heme-Copper Oxidases

Sun Hee Kim,[†] Constantino Aznar,[†] Marcin Brynda,[†] Louis A. "Pete" Silks,[‡] Ryszard Michalczyk,[‡] Clifford J. Unkefer,[‡] William H. Woodruff,*[,§] and R. David Britt*[,†]

Contribution from the Department of Chemistry, University of California, Davis, California 95616; National Stable Isotope Resource, Bioscience Division, Mail Stop G-578, LANL, Los Alamos, New Mexico 87545; and National Stable Isotope Resource, Chemistry Division, C-SIC, Mail Stop J582 LANL, Los Alamos, New Mexico 87545

Received June 23, 2003; Revised Manuscript Received October 28, 2003; E-mail: rdbritt@ucdavis.edu

Abstract: We report CW-EPR, ESEEM, and structural NMR results, as well as DFT calculations, on model compounds relevant to the unusual cross-linked Tyr-His (YH) moiety at the active site of the heme-copper oxidases. CW-EPR spectra of an ^{15}N isotopically labeled 4-methyl-2-(4-methyl-imidazole-1-yl)-phenol radical are nearly identical to those of the natural abundance ^{14}N compound. We obtain good simulations of these EPR spectra without including hyperfine couplings to the nitrogen nuclei. This implies that the electron distribution of the radical is largely localized on the phenol ring with only a small amount of spin delocalized onto the nitrogens of the imidazole. Using three-pulse ESEEM spectroscopy, we have successfully detected the two imidazole ring nitrogens, one near the "exact cancellation" ESEEM condition and the other more weakly coupled. We assign these to the imino and amino nitrogens, respectively, based on DFT calculations performed on this radical species. The experimental results and the supporting density functional calculations clearly show that the imidazole substituent has only a minor effect on the electronic structure of the substituted phenol radical.

Introduction

The heme-copper oxidases constitute a "superfamily" of membrane-bound enzymes that serve as terminal electron acceptors in the respiration of many prokaryotes and essentially all higher organisms.[1] As such, these oxidases are responsible for more than 90% of the biological O_2 consumption on earth and approximately half of the energy of aerobic respiration. In the particular case of the cytochrome c oxidases, the most widespread subclass of heme-copper oxidases, electrons donated from cytochrome c are used to reduce O_2 to H_2O. Cytochrome c oxidase contains two heme moieties, heme a and heme a_3, a dimeric copper center, Cu_A, and a mononuclear copper, Cu_B. Heme a_3 is associated with the proximal Cu_B in the heme-copper "binuclear" active site. O_2 reduction is thought to involve only the heme a_3 and Cu_B centers, with Cu_A and heme a serving sequentially as electron-transfer cofactors between cytochrome c and the binuclear catalytic site.

Recent X-ray structures of cytochrome c oxidase from the bovine heart mitochodria,[2,4] *Paracoccus denitrificans*,[3] and *Rhodobacter sphaeroides*[5] have shown the presence of a modified tyrosine close to the binuclear site (Y244, in bovine heart enzyme − the bovine residue numbers are used herein unless otherwise stated). This tyrosine is covalently cross-linked (see Figure 1) to a histidine residue, H240, which is also a ligand of Cu_B. This unusual ring−ring cross-link suggests a post-translation radical coupling mechanism during early O_2 turnover, and it has been speculated that the cross-linked tyrosine-histidine (YH) moiety could, at least under some conditions, serve as a reductant in the O−O bond cleavage chemistry. Specifically, in such a model, oxidation of the Fe_{a3}^{2+}/Cu_B^{+} binuclear center to the $Fe_{a3}^{4+}{=}O$, $OH{-}Cu_B^{2+}$ form provides three of the required electrons, and an oxidation of the YH species provides the fourth, resulting in radical formation.[6−8] Concerted electron and proton transfer from YH could provide an additional impetus for O−O bond cleavage and/or energy transduction by proton translocation. The cross-linking with histidine may act to alter

[†] University of California.
[‡] National Stable Isotope Resource.
[§] National Stable Isotope Resource, Chemistry Division.

(1) (a) Ferguson-Miller, S.; Babcock, G. T. *Chem. Rev.* **1996**, *96*, 2889−2907. (b) Malstrom, B. G. *J. Bioinorg. Chem.* **1998**, *3*, 339−343.
(2) Tsukihara, T.; Aoyama, H.; Yamashita, E.; Tomizaki, T.; Yamaguchi, H.; Shinzawa-Itoh, K.; Nakashima, R.; Yaono, R.; Yoshikawa, S. *Science* **1995**, *269*, 1069−1074.
(3) Ostermeier, C.; Harrenga, A.; Ermler, U.; Michel, H. *Proc. Natl. Acad. Sci. U.S.A.* **1997**, *94*, 10547−10553.
(4) Yoshikawa, S.; Shinzawa-Itoh, K.; Nakashima, R.; Yaono, R.; Yamashita, E.; Inpue, N.; Yao, M.; Fei, M. J.; Libeu, C. P.; Mizushima, T.; Yamaguchi, H.; Tomozaki, T.; Tsukihara, T. *Science* **1998**, *280*, 1723−1729.
(5) Svensson-Ek, M.; Abramson, J.; Larsson, G.; Tornroth, S.; Brzezinski, P.; Iwata, S. *J. Mol. Biol.* **2002**, *321*, 329−339.
(6) Proshlyakov, D. A.; Pressler, M. A.; Babcock, G. T. *Proc. Natl. Acad. Sci. U.S.A.* **1998**, *95*, 8020−8025.
(7) Gennis, R. B. *Biochim. Biophys. Acta* **1998**, *1365*, 241−248.
(8) Michel, H. *Proc. Natl. Acad. Sci. U.S.A.* **1998**, *95*, 12819−12824.

10.1021/ja0303743 CCC: $27.50

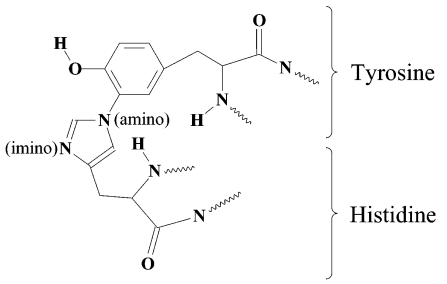

Figure 1. Covalently ring-linked tyrosine-histidine structure in the heme-copper oxidase.

the oxidation potential or pK_a of the tyrosine to facilitate its participation in these reactions.[6]

A radical EPR signal has been observed in cytochrome c oxidase following reaction with hydrogen peroxide.[9−11] This EPR signal was alternately identified as arising from a tyrosine[10] or a tryptophan radical.[11] However, such hydrogen peroxide produced radicals have been observed in several heme proteins, and this is believed to be due to oxidation of amino acids promoted by the reaction of hydrogen peroxide with the heme iron.[9] Thus, the identity of this cytochrome c oxidase radical species and its catalytic relevance are unclear. Recently, Proshlyakov and co-workers reported evidence suggesting that the cross-linked Y244−H240 is oxidized to a radical form. They reported that a substantial increase in the radioactive labeling of a Y244−H240 fragment arises from the reaction between radioactive $^{125}I^-$ and this radical.[12] This assignment still remains to be confirmed by direct spectroscopic observation of the proposed tyrosine-histidine radical. However, the mechanistic aspects of this proposal are appealing, and therefore it is important to determine the electronic structure of such cross-linked tyrosine-histidine radicals using both experimental and quantum mechanical approaches.

Here we report the characterization of a model of the cross-linked YH moiety by structural NMR (for the reduced diamagnetic form) and by CW-EPR and electron spin−echo envelope modulation (ESEEM) spectroscopies (for the oxidized radical form). The NMR studies, along with parallel X-ray crystallography work, establish the solution structures of the YH model and its synthetic precursors, while the paramagnetic spectroscopies establish the degree to which the histidine cross-linkage perturbs the tyrosine radical electronic structure. In addition, density functional calculations are employed to compare with the experimental results. The model that we have chosen for the YH moiety in the enzymes, 4-methyl-2-(4-methyl-imidazole-1-yl)-phenol, embodies the minimum essential features of YH, namely the phenol and imidazole rings covalently linked at the relevant positions and the methylene groups of the tyrosine and histidine side chains mimicked by methyl substituents on the rings. The high-yield synthetic procedure (vide infra) allows efficient incorporation of ^{15}N-labeled imidazole derivatives to test the extent of inter-ring spin delocalization in the radical and to facilitate assignments of vibrational spectra. Both experimental and calculation results

Scheme 1

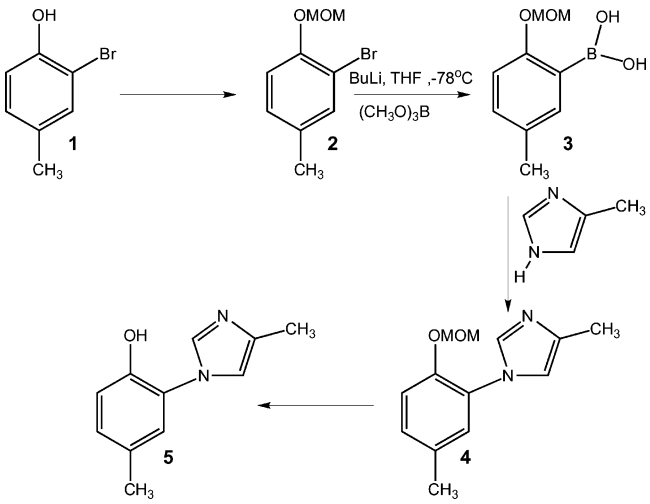

on these model compounds will provide bases for comparative studies with the analogous cross-linked YH species in the enzymes.

Materials and Methods

Synthesis of 2-(4-Methyl-1*H*-imidazol-1-yl)-4-methyl Phenol. We have reported the synthesis of the YH model 2-(4-methyl-1*H*-imidazol-1-yl)-4-methyl phenol **5** outlined in Scheme 1.[13] Briefly, 2-bromophenol **1** was converted to the corresponding MOM-ether **2**. The bromide was transmetalated, and the resulting carbanion was trapped with trimethylborate. Hydrolysis yielded the boronic acid derivative acid **3**. A copper promoted coupling of **3** with 4-methylimidazole gave 2-(4-methyl-1*H*-imidazol-1-yl)-1-(methoxymethoxy)-4-methyl benzene **4** was followed by the removal of the MOM-protecting group to give the YH model **5**. The doubly labeled ^{15}N isotopomer of **5** was prepared by substituting 4-methyl[$^{15}N_2$]imidazole for methylimidazole in Scheme 1. 4-methyl-[$^{15}N_2$]imidazole was provided by the National Stable Isotope Resource and prepared by treatment of 4-chloromethyl[$^{15}N_2$]imidazole[14] with Raney nickel.

EPR Spectroscopy. A 10 mM solution of each compound was prepared in 40% NaOH/H_2O, loaded into a EPR quartz tube, deoxygenated by bubbling with argon, and slowly frozen in liquid nitrogen. The neutral radical form of each compound was generated by irradiation of the samples for 2 min with the full spectrum of a mercury arc lamp at 77 K. CW-EPR spectra were collected at a temperature of 70 K, or between 7 and 70 K for variable temperature experiments, using a Bruker ECS 106 X-band CW-EPR spectrometer equipped with an Oxford ESR900 liquid helium cryostat and an ITC503 temperature controller. Low microwave power (10 μW) was used to prevent saturation of the signal. ESEEM spectra were collected at a temperature of 4.2 K with a laboratory-built pulsed EPR spectrometer.[15] Three-pulse time domain ESEEM experiments were performed by incrementing T in the stimulated echo sequence: $\pi/2 - \tau - \pi/2 - T - \pi/2$-stimulated echo. A cosine Fourier backfill procedure was used to reconstruct the instrumental dead time for all three-pulse data in order to generate the final displayed Fourier transforms.[16] The CW-EPR simulations were performed with a program using the methodology described in ref 17, which includes the effects of anisotropic hyperfine

(9) Fabian, M.; Palmer, G. *Biochemistry* **1995**, *34*, 13802−13810.
(10) MacMillan, F.; Kannt, A.; Behr, J.; Prisner, T.; Michel, H. *Biochemistry* **1999**, *38*, 9179−9184.
(11) Rigby, S. E.; Junemann, S.; Rich, P. R.; Heathcote, P. *Biochemistry* **2000**, *39*, 5921−5928.
(12) Proshlakov, D. A.; Pressler, M. A.; Demaso, A.; Leykam, J. F.; DeWitt, D. L.; Babcock, G. T. *Science* **2000**, *290*, 1588−1591.
(13) Tomson, F.; Bailey, J. A.; Gennis, R. B.; Unkefer, C. J.; Li, Z. H.; Silks, L. A.; Martinez, R. A.; Donohoe, R. J.; Dyer, R. B.; Woodruff, W. H. *Biochemistry* **2002**, *41*, 14383−14390.
(14) Silks, L. A.; Dunkle, E.; Unkefer, C. J.; Sudmeier, J. L.; Butler, M.; Bachovchin, W. W. *J. Labelled Compd. Radiopharm.* **1995**, *36*, 947−951.
(15) Sturgeon, B. E.; Britt, R. D. *Rev. Sci. Instrum.* **1992**, *63*, 2187−2192.
(16) Mims, W. B. *J. Magn. Reson.* **1984**, *59*, 291−306.
(17) Brok, M.; Babcock, G. T.; De Groot, A.; Hoff, A. J. *J. Magn. Reson.* **1986**, *70*, 368−378

and g matrices. ESEEM simulations were performed for the electron spin $S = {}^1/_2$ and nuclear spin $I = 1$ case using numerical diagonalization of the spin Hamiltonian as previously described[18] and for the $S = {}^1/_2$, $I = {}^1/_2$ case using another simulation program kindly provided by Professor Kurt Warncke.

Quantum Mechanical Calculations. DFT calculations were carried out using the GAUSSIAN 98 package,[19] and the representations of the molecular structures and molecular orbitals were generated with the MOLEKEL program.[20] To calculate the electronic structure and spectroscopic properties of our model system, full optimizations of the geometries were performed with the hybrid B3LYP functional, including Becke's three-parameter nonlocal exchange potential and the nonlocal correlation functional of Lee−Yang−Parr, for both diamagnetic and paramagnetic molecules in gaseous phase. For all the calculations, a triple-ζ 6-311++g basis set extended with diffuse functions was used. The optimized geometries were verified for the minima by careful analysis of the calculated vibrational frequencies (second derivative of the energy). The anisotropic coupling tensors and isotropic Fermi contact couplings were also computed for the neutral radical. Additionally, for the sake of consistence, the EPR parameters on the neutral radical were recalculated with the triple-ζ EPR-III basis set of Barone et al.,[21] which better describes the region far from nuclei covered by the unpaired electron, and which is especially suitable for the calculation of the isotropic hyperfine couplings. The electric field gradient (EFG) tensors were calculated for the paramagnetic molecules in order to estimate the NQR coupling constants for the imidazole nitrogens. The calculated traceless EFG tensor elements in Cartesian coordinates are related to the quadrupolar coupling constant C_q by

$$C_q = e^2 Q \langle q_{zz} \rangle / h$$

and the asymmetry parameter η is defined according to

$$\eta = \frac{\langle q_{xx} \rangle - \langle q_{yy} \rangle}{\langle q_{zz} \rangle}$$

where $e\langle q_{xx}\rangle$, $e\langle q_{yy}\rangle$, and $e\langle q_{zz}\rangle$ are the principal components of the electric field gradient tensor. To convert the $\langle q_{zz}\rangle$ output from atomic units (au) into the ^{14}N quadrupolar coupling constant, we used a value of $Q = 20.44(3) \times 10^{-31}$ m^2, recently chosen in accurate DFT calculations of NQC parameters in imidazole derivatives by Torrent et al.[22]

Results

Several routes to models of the YH structure have been reported.[23,24] Each of the routes is based on a copper mediated coupling of the imidazole and phenol ring systems. As discussed below, we designed a minimal model compound with the molecular characteristics that would allow realistic interpretation of spectroscopic features resulting from the YH structure in the cytochrome oxidases. Our YH model **5** shown in Scheme 1 and Figure 2 contains 4-methylimidazole and *p*-cresol substructures covalently linked between N(1) of the imidazole ring and the ortho carbon (C2) of the phenol ring. This link mimics the His N−C Tyr bond in the oxidases, and the methyl groups mimic the β-carbons of His and Tyr. The regiochemistry of the model compound was confirmed by a ^{1}H-NOE study and by X-ray crystallography.

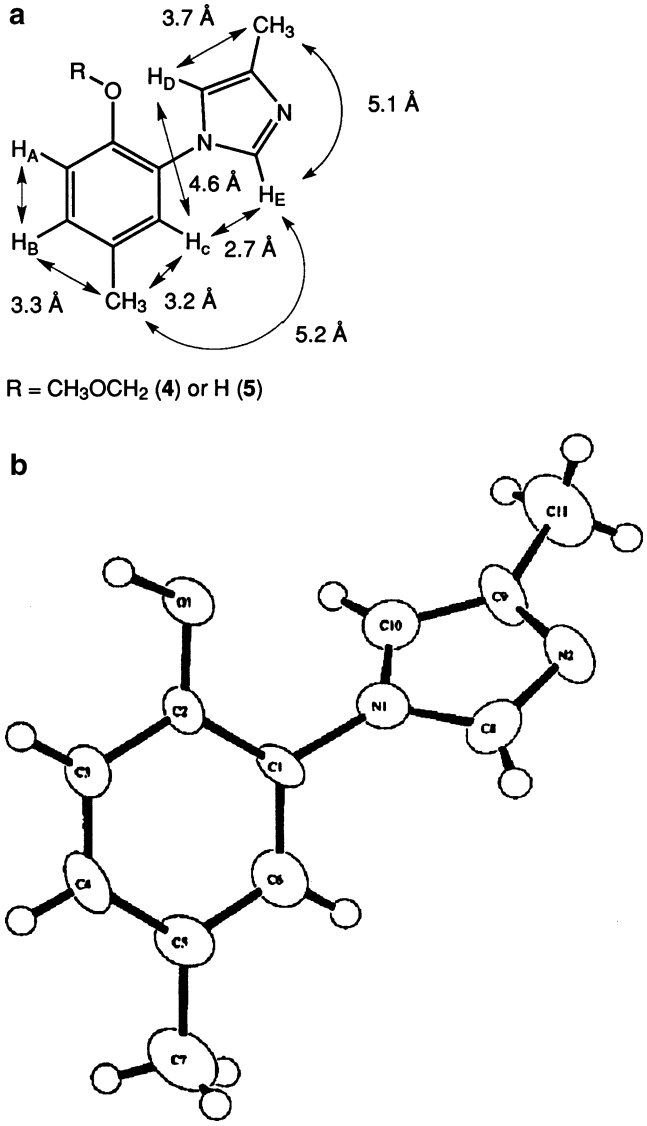

Figure 2. NOE derived distances of **4** and **5** and ORTEP drawing of the crystal structure of **5**.

Structural NMR. The regiochemistry of **4** and **5** (Scheme 1) were firmly established by NOE experiments on both products and by a crystal structure of **5**. Figure 2 illustrates the NOE derived distances for **4** and **5** and an ORTEP drawing of the crystal structure of **5**. The observed strong NOE between H_C and H_E and the lack of an NOE between the imidazole methyl group and H_C indicated the coupling reaction yielded the less sterically hindered regioisomer of **4**. Both the NOE and the crystal structure of **5** showed that the final product has the same regiochemistry. Our efforts to observe or isolate the other

(18) Britt, R. D.; Zimmermann, J.-L.; Sauer, K.; Klein, M. P. *J. Am. Chem. Soc.* **1989**, *111*, 3522−3532.
(19) Frisch, M. J.; Trucks, G. W.; Schlegel, H. B.; Scuseria, G. E.; Robb, M. A.; Cheeseman, J. R.; Zakrzewski, V. G.; Montgomery, J. A., Jr.; Stratmann, R. E.; Burant, J. C.; Dapprich, S.; Millam, J. M.; Daniels, A. D.; Kudin, K. N.; Strain, M. C.; Farkas, O.; Tomasi, J.; Barone, V.; Cossi, M.; Cammi, R.; Mennucci, B.; Pomeli, C.; Adamo, C.; Clifford, S.; Ochterski, J.; Petersson, G. A.; Ayala, P. Y.; Cui, Q.; Morokuma, K.; Malick, D. K.; Rabuck, A. D.; Raghavachari, K.; Foresman, J. B.; Ciolowski, J.; Ortiz, J. V.; Baboul, A. G.; Stefanov, B. B.; Liu, G.; Liashenko, A.; Piskorz, P.; Komaromi, I.; Gomperts, R.; Martin, R. L.; Fox, D. J.; Keith, T.; Al-Laham, M. A.; Peng, C. Y.; Nanayakkara, A.; Gonzalez, C.; Challacombe, M.; Gill, P. M. W.; Johnson, B.; Chen, W.; Wong, M. W.; Andres, J. L.; Head-Gordon, M.; Reploge, E. S.; Pople, J. A. *Gaussian 98*, revision A.7; Gaussian, Inc.: Pittsburgh, PA, 1998.
(20) Flukiger, P.; Luthi, H. P.; Portmann, S.; Weber, J. *MOLEKEL 4.3*; Swiss Center for Scientific Computing: Manno (Switzerland), 2000−2002.
(21) Barone, V. *Theor. Chim. Acta* **1995**, *91*, 113−128.
(22) Torrent, M.; Musaev, D. G.; Morokuma, K. *J. Phys. Chem. B* **1999**, *103*, 8618−8627.
(23) McCauley, K. M.; Vrtis, J. M.; Dupont, J.; van der Donk W. A. *J. Am. Chem. Soc.* **2000**, *122*, 2403−2404.
(24) Cappuccio, J. A.; Ayala, I.; Elliott, G. I.; Szundi, I.; Lewis, J.; Konopeiski, J. P.; Barry, B. A.; Einarsdottir, O. *J. Am. Chem. Soc.* **2002**, *124*, 1750−1760.

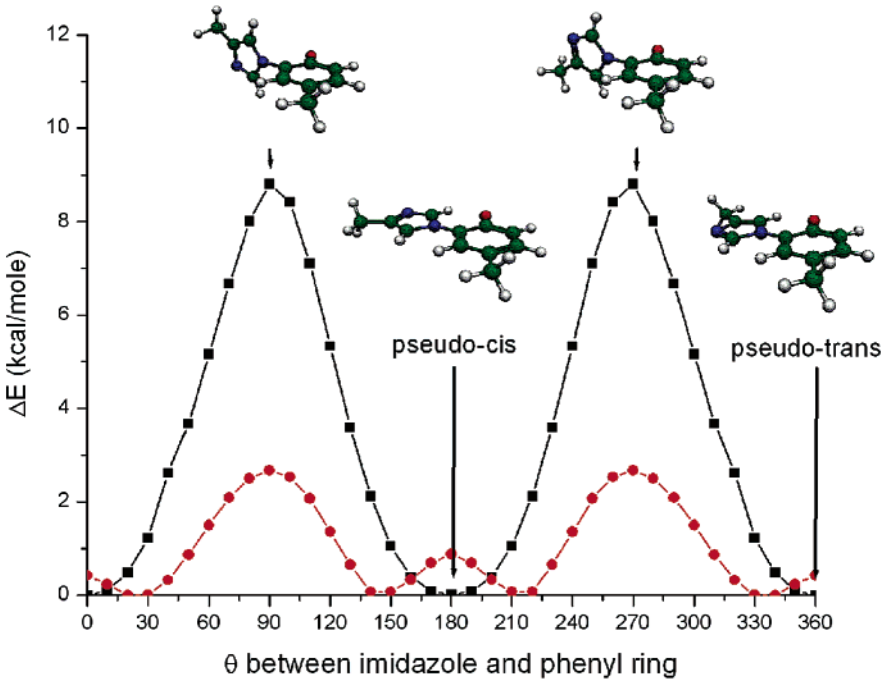

Figure 3. Rotational barriers calculated by DFT for radical (a - ■) and neutral (b - ●) forms of **5**. Calculations were made at B3LYP level with the 3-21g* basis set. Full relaxation of the geometry was allowed at every fixed θ angle (θ = angle between phenyl and imidazole ring).

regioisomer failed. In addition, lack of an NOE between the H_D proton of the imidazole and H_C indicates hindered rotation around the imidazole-aryl C−N bond. In addition to the dominating methyl resonances attributable to the rotamer of **5** (Figure 2), there are two small methyl resonances with a 30−35-fold lower intensity. These small resonances are present in the ^{1}H NMR spectra of all of our preparations of **5**. These small resonances may represent methyl groups of the other possible rotamer and its rotation in a slow chemical exchange regime. These data are consistent with hindered rotation around the C−N bond with bond rotamers present in solution in the ratio of 30:1 with the dominating rotamer of **5** pictured in Figure 2.

The DFT geometry optimization of compound **4** leads to two conformers (restricted rotation around the imidazole-aryl C−N bond giving rise to two distinguishable conformations with the imidazole methyl group "pseudo-cis" or "pseudo-trans" versus the methyl group on the phenol ring). The pseudo-cis rotamer has a slightly lower energy than the pseudo-trans rotational isomer (ΔE = 0.07 kcal/mol). The optimized pseudo-trans structure shows the expected arrangement of the −O−CH_2−O−Me fragment, close to the H_D proton of the imidazole ring.

The geometry of compound **5** is consistent with the structural data from the crystal structure (Figure 2). As in the case of **4**, two rotamer structures were optimized, leading to the energetically preferential pseudo-cis conformation (ΔE = 0.03 kcal/mol). As demonstrated by the NOE experiments and X-ray diffraction, **4** exists in solution (and correspondingly **5** in crystalline form) as the pseudo-trans rotamer. The energy difference between the DFT optimized structure of pseudo-trans and pseudo-cis rotamers for **4**, **5**, and **R5** is very small (of the order of zero-point vibrational energy). However, in analogy with **4** and **5**, we assume that **R5** in frozen solutions is in the pseudo-trans conformation and consequently present the spin density analysis on this specific conformation.

The optimized pseudo-trans structures of **4** and **5** are compatible with the NMR studies in solution. There is a reasonable fit between the interproton distances calculated from the DFT optimized structure of **4** and those observed from the NOESY experiments, except when looking at the MOM protecting group. These distances are most affected by spin diffusion of magnetization between CH_2 and CH_3. This would cause distances from other protons to the CH_2 group to appear longer and distances to the CH_3 group appear shorter than their actual values. The differences may also include effects of the rotation of the −CH_2−O−CH_3 group and distance averaging.

The geometry of the 2-(4-methyl-1*H*-imidazol-1-yl)-4-methyl phenoxy radical **R5** was optimized for both conformational pseudo-cis and pseudo-trans states. As in the case of the diamagnetic molecule, the pseudo-cis rotamer is characterized by a very slightly lower energy (ΔE = 0.08 kcal/mol). It is worth noting that the angle between the two planes containing phenol and imidazole ring (θ), respectively, passes from θ = 47.6 for **4**, θ = 42.6 for **5**, to a planar structure in the case of **R5** (θ = 0.1).

To check to what extent the conformation of the **5** is affected by the creation of its radical form, we have performed an additional set of calculations in order to estimate the barrier to rotation for both neutral and radical **5**. Figure 3 shows the rotational barriers calculated by DFT. For both radical and neutral forms, the maximum of the barrier appears when the plane containing the phenyl is normal to the plane containing the imidazole ring. A possible explanation of the shape of the barrier is that the main interaction in this particular system occurs between the oxygen atom and one (or the other, for the other rotamer) of the imidazole hydrogens. The fact that the maximum of the energy is found at 90° suggests that at this point the molecule is in the less energetically preferable conformation (the longest distance between imidazole protons

and O). By approaching one of the imidazole protons to the oxygen atom, the energy is lowered by about 9 kcal/mol in the radical form of **5**. This same maximum is found for the neutral molecule, but this time the minimum energy structure is found at an "intermediate" angle between 0° and 90° (42.6°). This is probably due to the repulsion between one (and, respectively, the other, for the other rotamer) of the imidazole protons and the proton of the hydroxyl group. The energy cannot be lowered anymore as much as in the radical form, and this is translated into a noticeably lower barrier height (about 3 kcal/mol). It is also worth noticing that both barriers are almost completely symmetrical and exhibit only two energetically equivalent minima (for the diamagnetic **5**, every pair of the overall four minimum energy conformations has the same energy and is fully symmetrical through the symmetry plane containing the phenol ring). This is an additional indication that the possible interactions arising from the imidazole imino nitrogen or the imidazole methyl group are negligible, and the only important ones involve the protons adjacent to the amino nitrogen on the imidazole ring (H connected to C8 and C9). Thus, the shape of calculated rotational barriers nicely illustrates a subtle interplay between different intramolecular interactions.

It is also interesting to compare the optimized geometries of **5** with the cross-linked YH site in cytochrome c oxidase enzyme. The conformation of the YH moiety in the crystal structure of BA3-Cytochrome oxidase from *Thermus thermophilus* corresponds to the lower energy DFT optimized rotamer (pseudo-cis conformation), and the angle between the phenol and imidazole rings is very close to that found in the DFT optimized geometry of the model complex (44° and 42.6°, respectively). The main difference between the two structures lies in the fact that, whereas in the DFT optimized structure the phenyl-imidazole bond is coplanar with the imidazole ring, in the enzyme site a slight pyramidality is observed for the imino nitrogen of the imidazole ring (the phenyl-imidazole bond makes an angle of 31° with the imidazole plane). Finally, the noticeable difference in the cycle−cycle (phenyl-imidazole) angle between the optimized geometries of the neutral **5** and the radical form suggests that a potential conformational switch is coupled to radical formation in the peptide macrocycle structure of the YH site in the enzyme.

CW-EPR. We have performed CW-EPR spectroscopy on the neutral radical forms of *p*-cresol, unlabeled **5**, and ^{15}N labeled ^{15}**N-5** YH model compounds. Figure 4 shows the X-band CW-EPR spectra of the UV generated radicals (solid lines) along with simulations (dotted lines). The *p*-cresol radical gives rise to a well resolved 10 line spectrum (Figure 4a) resulting from large hyperfine couplings to the methyl protons and a smaller coupling to the two ortho ring protons. The two weakly coupled meta ring protons contribute only to line broadening. The CW-EPR spectrum of **5** (Figure 4b), the compound in which an imidazole group replaces one of the ortho ring protons on *p*-cresol, shows that substitution of an imidazole group at the ortho position eliminates the moderately strong coupling to the proton that was in this position, resulting in a narrower EPR spectral width than observed for *p*-cresol.[25] To directly probe

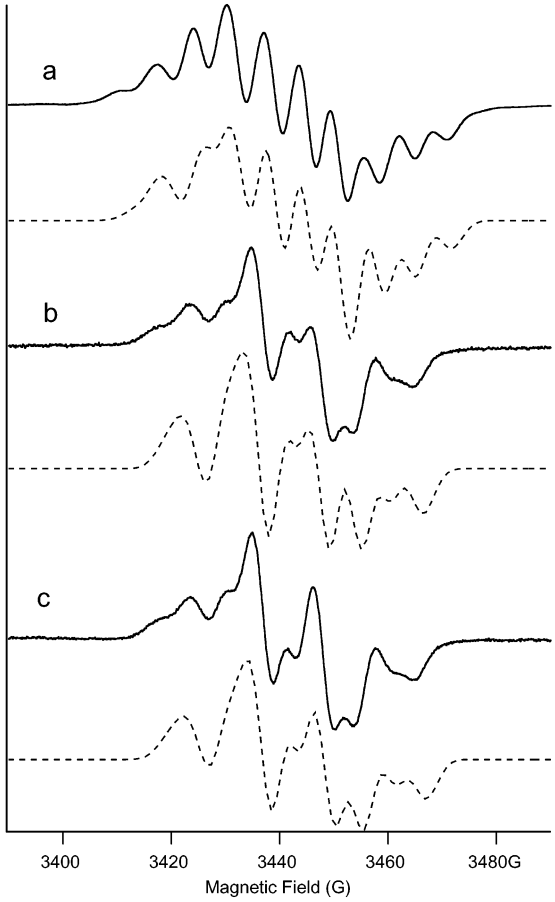

Figure 4. CW-EPR spectra of the radical form of (a) *p*-cresol, (b) unlabeled compound **5**, and (c) ^{15}N labeled compound ^{15}**N-5**. Each dotted line displays the simulations of the spectra in part a and parts b and c. Experimental parameters: CW-EPR spectrometer, Bruker ECS-106; temperature, 70 K; microwave frequency, 9.68 GHz; microwave power, 10 μW; modulation amplitude, 1 G. The following parameters were used in the simulation: (a) three equivalent β-protons (A_{xx} = 37.6 MHz, A_{yy} = 33.6 MHz, A_{zz} = 33.6 MHz), ϕ = 75°; two ortho protons (A_{xx} = 27.3 MHz, A_{yy} = 9.1 MHz, A_{zz} = 18.2 MHz), ϕ = 57°; two meta protons (A_{xx} = 7.14 MHz, A_{yy} = 2.24 MHz, A_{zz} = 4.56 MHz); ϕ = 35°, g-tensors (g_{xx} = 2.0065, g_{yy} = 2.0050, g_{zz} = 2.0023); line width 2.1 G; (b, c) three equivalent β-protons (A_{xx} = 33.6 MHz, A_{yy} = 31.6 MHz, A_{zz} = 31.6 MHz), ϕ = 60°; one ortho proton (A_{xx} = 24.3 MHz, A_{yy} = 6.1 MHz, A_{zz} = 16.2 MHz for part b, A_{zz} = 15.2 MHz for part c), ϕ = 62°; two meta protons (A_{xx} = 4.14 MHz, A_{yy} = 0.24 MHz, A_{zz} = 1.76 MHz), ϕ = 45°; g-tensors (g_{xx} = 2.0065, g_{yy} = 2.0050, g_{zz} = 2.0023); line width 2.5 G. ϕ represents a rotation of the hyperfine components, defined in the molecular axis system, to the g-axes frame.

the degree of hyperfine interactions with the two nitrogens of the linked imidazole, we also obtained the CW-EPR spectrum of the radical form of ^{15}**N-5** (Figure 4c). This spectrum shows very little line shape difference when compared that of the natural abundance nitrogen form of this radical (Figure 4b). It should be noted that the only difference between the CW-EPR spectra of **5** and ^{15}**N-5** is the line intensity in the region from 3438 to 3452 G. However, overall line widths and shapes are almost identical between two spectra. The simulations of the radical forms of this YH dimer model compounds proved that the line shape in the region from 3438 to 3452 G is quite sensitive to variation of the hyperfine constants and angle ϕ. The simulations of **5** and ^{15}**N-5** only differ in the hyperfine component A_{zz} of an ortho proton by 1 MHz.

Overall, we can obtain good simulations of the EPR spectra of compounds **5** and ^{15}**N-5** using only hyperfine couplings to

(25) Recently van der Donk and co-workers[23] reported the EPR signal of the 2-imidazole-1-yl-4-methylphenol radical. The overall line width and line shape of the EPR signal we observed here are similar to those reported. However, the EPR spectrum reported here differs from a very recent result by Cappuccio et al.[24] of the radical form of a cross-linked histidine-phenol due to the absence of methyl protons of the compound.

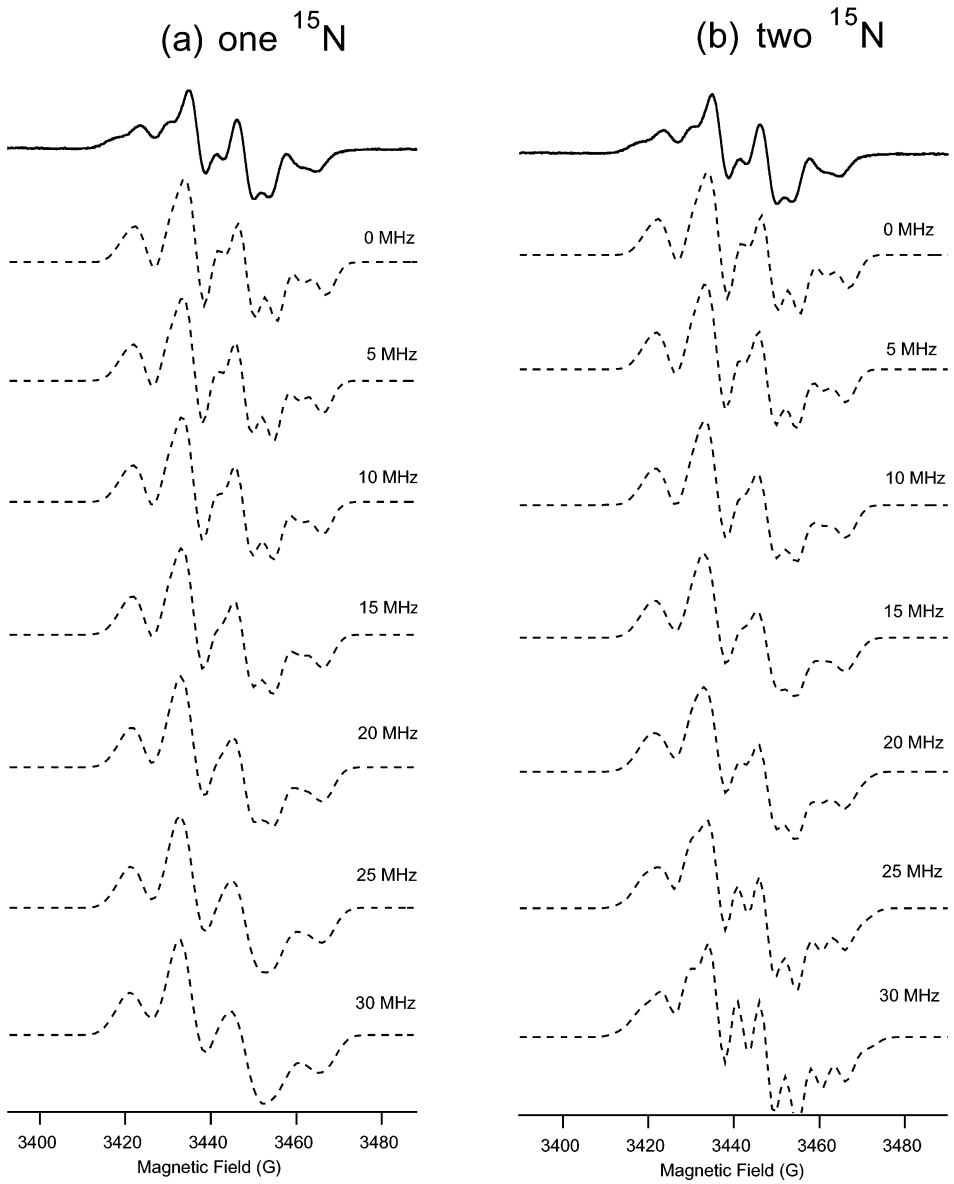

Figure 5. Simulated EPR spectra of the ^{15}N labeled compound ^{15}**N-5** with different hyperfine values for one ^{15}N and two equivalent ^{15}N nuclei, respectively. The other simulation parameters are the same as those in Figure 4b,c.

the methyl and ring protons, without adding hyperfine couplings to the ^{14}N or ^{15}N nitrogen nuclei. This indicates that there are only small hyperfine couplings to the imidazole ring nitrogens. We note that there is a slight difference in the EPR line shapes of the ^{14}N and ^{15}N radical samples at the center of the spectrum (the 3438−3452 G region), but even very small changes in proton couplings affect this region. For example, the differences in this region are adequately simulated with a 1 MHz difference in the A_{zz} component of an ortho proton (Figure 4b,c and simulations), whereas we have been less successful in simulating an ^{14}N/^{15}N induced change that affects only this central region of the spectrum. We can examine the effects of increased ^{14}N/^{15}N hyperfine couplings in simulations and their match to the observed spectra. Figure 5 shows simulated EPR spectra of compound ^{15}**N-5** as a function of a varied hyperfine coupling parameter for the two limiting cases of one ^{15}N nucleus (Figure 5a) or two equivalent ^{15}N nuclei (Figure 5b). Large nitrogen hyperfine coupling values broaden the resolved features. Figure 6 shows the plot of the standard deviation between the experimental spectrum and the simulated spectra as a function of the hyperfine coupling constant(s) for one ^{15}N or two equivalent ^{15}N nuclei. These results suggest an upper limit for the ^{15}N coupling to be approximately 20 MHz for either limiting case.

The variable temperature (VT) spectra of the ^{15}**N-5** radical (Figure 7) reveal a dramatic change in the line shape between 7 K and about 30 K. This is indeed expected, since the methyl group attached to the phenyl group undergoes restricted rotational dynamics. It has been shown that in the temperature range of 4−40 K, the internal motions of methyl rotors of R−C$^{\bullet}$−CH_3-type radicals are slowed or even completely blocked.[26] When examining the VT spectra of the ^{15}**N-5** radical, it is seen that below 30 K the intensity of the two central lines decreases, and a third line arises between the two most intense transitions. As expected, above 30 K the methyl group freely rotates and the three equivalent methyl protons contribute to

(26) Sornes, A. R.; Benetis, N. P.; Erickson, R.; Mahgoub, A. S.; Eberson, L.; Lund, A. *J. Phys. Chem. A* **1997**, *101*, 8987−8994.

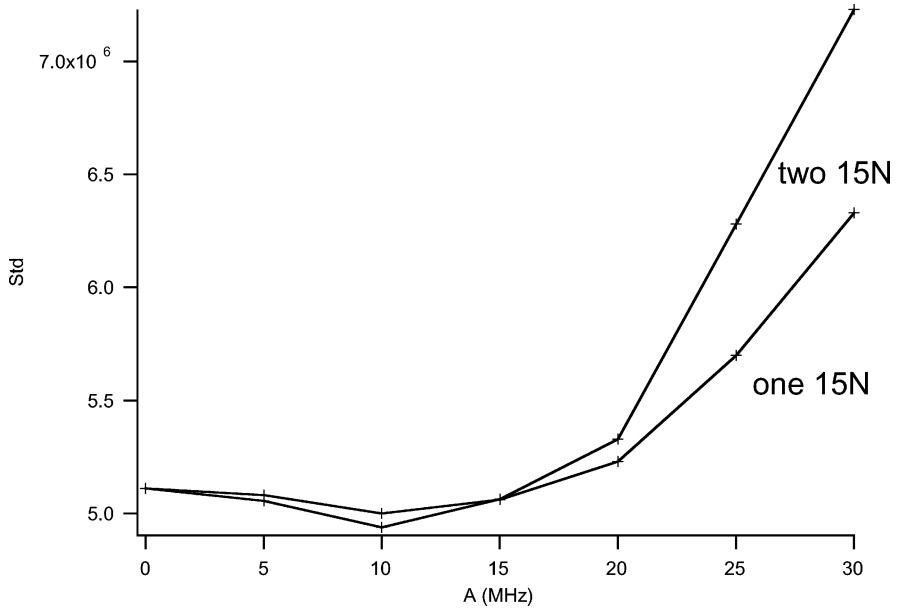

Figure 6. Plot of the standard deviation between experimental spectrum and the simulated spectrum as a function of the hyperfine coupling constant. The two curves correspond to the one and two ^{15}N cases, respectively.

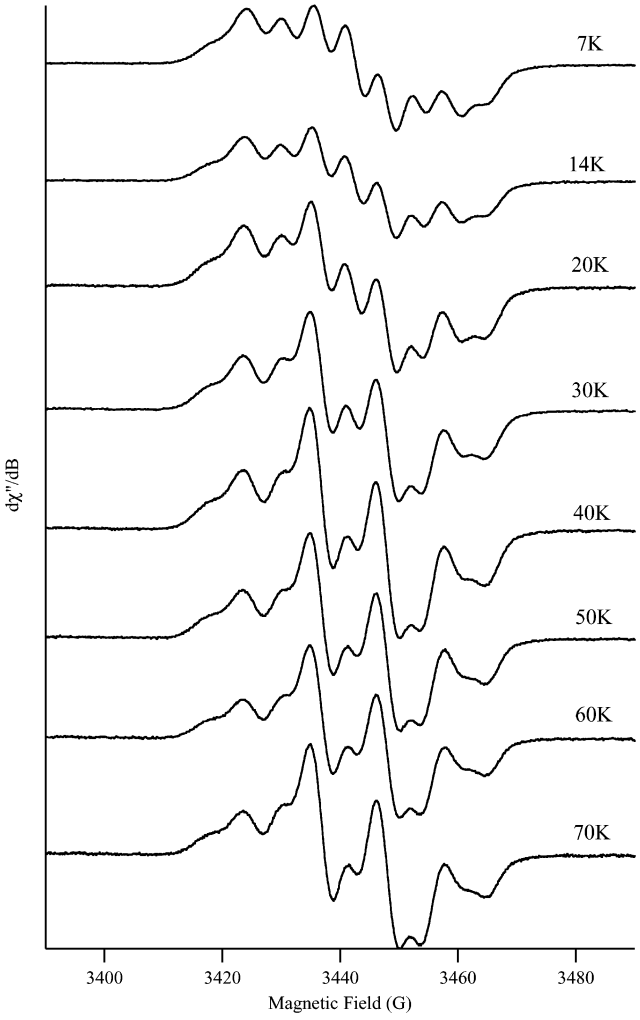

Figure 7. Variable temperature CW-EPR spectra of the radical form of the ^{15}**N-5** compound.

the spectrum with the same A_{iso}, giving rise to the classical 1:3:3:1 pattern. When the temperature is decreased, the rotational motion is slowed and then blocked around 7 K. The equivalence of the three methyl protons is lost in this temperature range, and a 1:1:1:2:1:1:1 pattern is observed. It should be underlined that, in the frozen solution spectrum of ^{15}**N-5** radical, the phenolic ortho and meta protons contribute to the spectral broadening of the line shape. They should be thus taken into account in the line shape simulation. An experimental and DFT calculational investigation is in progress to understand the rotational dynamics of the CH_3 fragment and to estimate the energy barrier to rotation.

ESEEM. We have directly measured the weak imidazole nitrogen hyperfine couplings using the ESEEM spectroscopy technique, which is sensitive for the detection of weakly coupled nuclei. Figure 8 shows three-pulse ESEEM Fourier transform spectra of the *p*-cresol, compound **5**, and ^{15}**N-5** radicals, respectively. As expected, three-pulse ESEEM of the *p*-cresol radical (Figure 8a) detects no ^{14}N frequencies.[27] Figure 8b shows the three-pulse ESEEM frequency domain spectrum of the ^{15}**N-5** radical, which is completely distinct from the spectrum of the unlabeled natural abundance ^{14}N radical **5** shown in Figure 8d. This clearly demonstrates that the three-pulse ESEEM peaks shown in Figure 8b and 8d, respectively, arise from the ^{15}N and ^{14}N nitrogens of the two compounds.[27] The 2.9 MHz peak in the frequency domain spectrum of the ^{15}**N-5** radical is close to twice the ^{15}N Larmor frequency at this field ($\nu_n = 1.45$ MHz), which indicates that this peak results from an ^{15}N nucleus (designated N_A) with nearly identical hyperfine and external fields. This "exact cancellation" limit is well-known for giving rise to appreciable modulation for $I = {}^1/_2$ ^{15}N or $I = 1$ ^{14}N nuclei.[28] Therefore using the first-order perturbation expression $\nu_\pm = |\nu_n \pm A/2|$, we can estimate the value of the hyperfine coupling constant $A(^{15}N)$ to be approximately 2.9 MHz [$A(^{14}N) = 2.1$ MHz, scaled by the ratio of the magnetic moments of the ^{14}N and ^{15}N nuclei]. We also observe a contribution at the

(27) Modulation from weakly coupled protons is suppressed by our selection of a τ value that is a multiple of the proton Larmor frequency.
(28) (a) Lai, A.; Flanagan, H. L.; Singel, D. J. *J. Chem. Phys.* **1988**, *89*, 7161−7166. (b) Flanagan, H. L.; Singel, D. J. *J. Chem. Phys.* **1987**, *87*, 5606−5616.

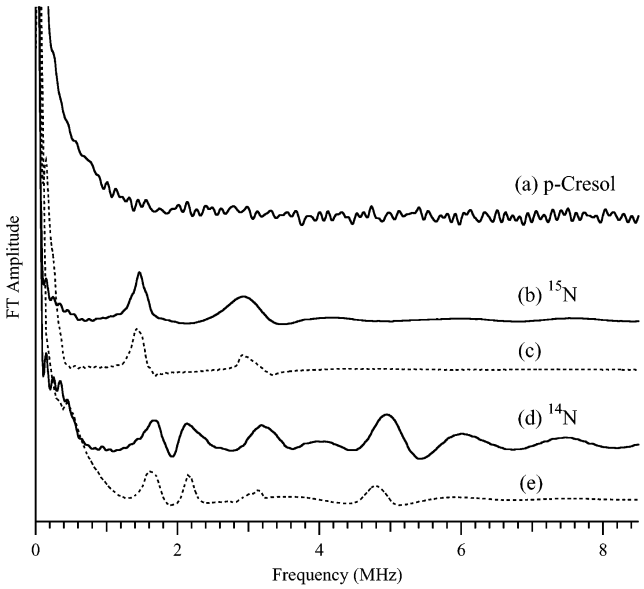

Figure 8. Three-pulse ESEEM Fourier transform spectra of the radical form of (a) *p*-cresol, (b) ^{15}N labeled compound ^{15}**N-5**, (c) a simulation of this ^{15}N ESEEM spectrum, (d) unlabeled compound **5**, and (e) a simulation of this ^{14}N ESEEM spectrum. Experimental parameters: microwave frequency = 9.422 GHz; B = 3366 G; τ = 279 ns; starting T = 81 ns; T increment = 40 ns; microwave power = 16 W; repetition rate = 50 Hz; $\pi/2$ pulse length = 15 ns; temperature = 4.2 K. (c) The simulation parameters for two ^{15}N nitrogens; A_{iso} = 3.2 MHz, A_{dip} = 0.4 MHz (N_A), A_{iso} = 0.01 MHz, A_{dip} = 0.3 MHz (N_B). (e) The simulation parameters for two ^{14}N nitrogens; A_{iso} = 2.3 MHz, A_{dip} = 0.1 MHz, e^2qQ = 2.5 MHz, and η = 0.32 (N_A) and A_{iso} = 0.005 MHz, A_{dip} = 0.20 MHz, e^2qQ = 2.24 MHz, and η = 0.905 (N_B).

Larmor frequency of 1.45 MHz arising from the other weakly coupled ^{15}N nucleus (designated N_B) of the imidazole ring.[29] The coupling constant $A(^{15}N)$ is close to zero for the weakly coupled N_B nitrogen. The simulation was carried out with these initial estimates for isotropic hyperfine coupling constants from the analytical expression. The ESEEM spectra of each nitrogens were first simulated separately and then combined using the product rule[30] to account for two nitrogen modulations since the modulation of two nuclei comes as the product of the two independent modulation patterns. The simulated ^{15}N ESEEM spectrum is shown in Figure 8c with A_{iso} = 3.2 MHz, A_{dip} = 0.4 MHz for N_A and A_{iso} = 0.01 MHz, A_{dip} = 0.3 MHz for N_B. The simulation accounts well for the frequencies, relative ampliude, and line widths of the ESEEM features. The simulated time-domain ESEEM spectra performed using two coupled nuclei, N_A and N_B, are also shown in Figure 9 (dotted lines). Figure 9a shows a comparison of the experimental and simulated time-domain three-pulse ESEEM spectra for the ^{15}N radical.

Given the ^{15}N ESEEM assignment of two nitrogens, N_A (near exact cancellation), and N_B (weakly coupled), can we find consistent simulation parameters for the natural abundance ^{14}N radical that give rise to good simulations to the more complex ^{14}N ESEEM spectrum?

For a nitrogen near exact cancellation (i.e., N_A), the ^{14}N ESEEM frequencies in a three-pulse experiment generally consist of the three possible "NQR" transitions (ν_0,ν_-,ν_+) between the three nuclear quadrupole sublevels at effectively zero field and a higher frequency "double quantum" $\Delta M_I = 2$ feature, ν_{dq}. We assign three NQR peaks at 0.48, 1.67, and 2.15 MHz plus a "double quantum" feature at 4.94 MHz to N_A, the ^{14}N near exact cancellation in Figure 8d. The hyperfine coupling constant A, the nuclear quadrupole coupling constant e^2qQ, and the quadrupole asymmetry parameter η can then be estimated using the following expressions:

$$\nu_0 = 2K\eta,\ \nu_- = K(3-\eta),\ \nu_+ = K(3+\eta),$$

$$\nu_{dq} = 2[(\nu_n + A/2)^2 + K^2(3+\eta^2)]^{1/2}, \text{ where } K = e^2qQ/4.$$

From these expressions, we estimate a hyperfine coupling of $A(^{14}N)$ = 2.4 MHz, in reasonably close agreement with the value $A(^{14}N)$ = 2.1 MHz for N_A obtained independently from the ^{15}N ESEEM analysis. These analysis also gives the values of e^2qQ = 2.55 MHz and η = 0.38. These initial estimates for nuclear quadrupole and isotropic hyperfine constants were used for the starting values for the three-pulse ESEEM FT simulation. The estimated values for e^2qQ and η were varied for the positions of the low-frequency components, and then hyperfine values were varied to obtain the correct position of the double quantum peak. The best simulation was produced with A_{iso} = 2.30 MHz, A_{dip} = 0.1 MHz, e^2qQ = 2.50 MHz, and η = 0.32.

The second nitrogen, N_B, is more weakly coupled. Away from exact cancellation, one often observes two major ^{14}N ESEEM peaks.[28b] To account for the peak at 3.18 MHz the simulation was obtained with ^{14}N parameters of A_{iso} = 0.005 MHz, A_{dip} = 0.20 MHz, e^2qQ = 2.24 MHz and η = 0.905. This provides an additional peak at 3.18 MHz, along with additional 1.6 MHz intensity. We use this set of parameters as a working assignment for N_B, the weakly coupled ^{14}N. The product of the two simulated ^{14}N modulation functions (Figure 9b) gives a Fourier transform spectrum (Figure 8e) in good agreement with the experimental spectrum (Figure 8d).

A direct comparison of the experimental ESEEM time domain spectra (solid lines) for the radical forms of ^{15}**N-5** and **5** with those obtained from the simulations (dotted lines) is shown in Figure 9. The depth of molulations in the ^{15}N three-pulse time domain data and simulation agrees well (Figure 9a), which shows that the CW-EPR and ESEEM are consistent in accounting for all coupled nitrogens in the model compound.

The situation is less straightforward for the more complicated ^{14}N case, in that to obtain a good simulation to the modulation pattern, the relative contributions of the two ^{14}N nuclei N_A and N_B were scaled. After scaling, we obtain a good match to experimental time and frequency domain spectra, but it is clear that experimental improvements, such as the use of the two-dimensional HYSCORE method,[31] or synthetic improvements, such as specifically ^{15}N-labeling one of the two imidazole nitrogens, are in order to further constrain simulations of this complicated situation with two inequivalent I = 1 nuclei. Both of these approaches are currently being pursued. It should be noted here that the three-pulse ESEEM experiments using different τ values revealed no other ESEEM features in both ^{14}N and ^{15}N even though there are peak intensity changes due

(29) We note here that weakly coupled nitrogen nuclei from proximal solute molecules are unlikely to contribute to ESEEM spectra, since, at a 10 mM concentration, approximately 0.0005 other solute molecules would be located within a distance of 6 Å or less, which is a good estimate of detectable distance for weakly coupled nitrogens in ESEEM experiments. Therefore, we can rule out detection of intermolecular nitrogen couplings.

(30) (a) Mims, W. B. *Phys. Rev. B* **1972**, *5*, 2409−2419. (b) Dikanov, S. A.; Shubin, A. A.; Parmon, V. N. *J. Magn. Reson.* **1981**, *42*, 474−487.

(31) Dikanov, S. A.; Bowman, M. K. *J. Magn. Reson., Ser. A* **1995**, *116*, 125−128.

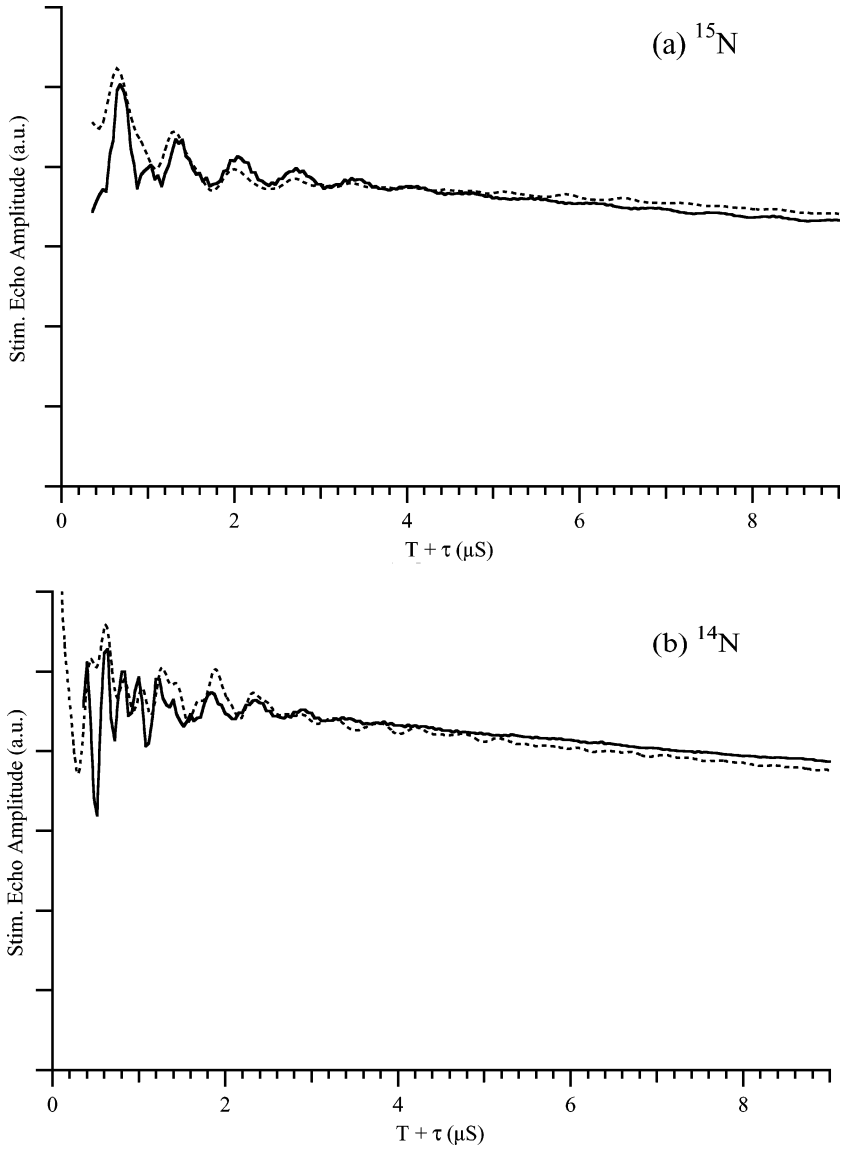

Figure 9. Comparison between the three-pulse ESEEM experimental spectra (solid lines) and the simulated time domain (dotted lines) for the ^{15}N (a) and the ^{14}N (b), respectively. The Fourier transformations of the simulated time domain are shown in Figure 8. To obtain a good simulation of an ^{14}N ESEEM spectrum, the relative contributions of the two ^{14}N nuclei, N_A and N_B, were scaled by $^1/_4$ and 4, respectively. See text for details.

to τ-suppression effects as expected (data not shown). Therefore, we, indeed, account for all ESEEM features arising from magnetically coupled ^{14}N and ^{15}N nuclei.

We conclude that the ESEEM spectroscopy and analysis for both ^{15}N and ^{14}N radical forms reveal both nitrogens of the imidazole substituent. Both nitrogens are relatively weakly coupled, which is why they are not observed directly in the CW EPR spectra. One nitrogen, designated N_A, has an appreciably larger hyperfine interaction than the second nitrogen, N_B. We do not currently have samples available with specific ^{15}N-labeling of amino vs imino nitrogens. However, DFT calculations can be used to help us map the ESEEM observed N_A and N_B nitrogens to the chemically distinct amino and imino nitrogens of the imidazole substituent (Figure 1).

DFT Calculations: Spin Distribution and Spectroscopic Parameters for Neutral Radical R5. Density functional theory (DFT) has been proven to be an accurate predictive tool, not only for the calculation of the molecular geometries but also for the computation of spectroscopic properties such as hyperfine coupling or quadrupolar coupling constants of organic molecules.[32] To support our experimental results and facilitate the assignment of the ESEEM signals to the specific nitrogens of the imidazole ring, we performed a set of DFT calculations on the neutral radical **R5**. The spin density, EPR, and NQR parameters were computed for the pseudo-trans rotamer of the model radical. The SOMO orbital of **R5** is represented in Figure 10 (gross spin−orbital population: $s = 0.02$, $p = 0.80$). The unpaired electron is strongly localized on the oxygen atom; a major part of the spin is also delocalized on the phenyl ring in a hybrid orbital. The electron spin distribution of the SOMO corresponds at first approximation to the positive unpaired ($\alpha-\beta$) spin density. The highest concentration of the net positive spin density is found on oxygen (positive spin density on oxygen $= 0.42$) and on phenolic carbons C1 (0.35), C3 (0.22), and C5 (0.35). A negative spin, induced by spin polarization, is found on carbons C2 (−0.08), C4 (−0.12), and C6 (−0.24). Consistent

(32) Arbuznikov, A. V.; Kaupp, M.; Malkin, V. G.; Reviakine, R.; Malkina, O. L. *Phys. Chem. Chem. Phys.* **2002**, *22*, 5467−5474.

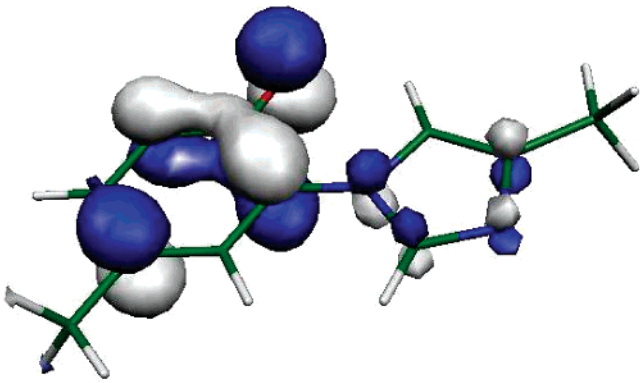

Figure 10. SOMO orbital of **R5** obtained from DFT calculations.

Table 1. EPR Parameters Calculated for **R5**[a]

nucleus	A_{iso}	τ_1	τ_2	τ_3
N_{amino}	0.2	−2.5	−2.2	4.7
N_{imino}	0.5	−1.0	−0.9	1.9
ortho-H	−14.1	−5.6	−2.2	7.9
meta$_1$-$H_{(im)}$	7.3	−2.9	−1.2	4.1
meta$_2$-H	5.1	−2.3	−0.1	2.4
phenol methyl H[b]	24.2	−1.7	−1.2	2.9

[a] Selected values of A_{iso} and τ [MHz] for nitrogen atoms and protons in **R5** calculated by DFT. [b] Values for methylic hydrogen were averaged over three protons in the methyl fragment.

with the experimental results, the spin density on the imidazole ring is very low (total spin density 0.09); for the two nitrogens, this spin density is less than 0.04 (0.017 for the imino nitrogen and 0.016 for the amino nitrogen).

The isotropic and anisotropic parts of the hyperfine coupling were calculated for the fully optimized structure of **R5**. The calculated values of the hyperfine coupling parameters for the imidazole nitrogens and some selected hydrogens in the pseudo-trans conformation of **R5** are presented in Table 1. The spin distribution is mirrored by the values of the hyperfine coupling constants of the hydrogen and nitrogen atoms. The *o*-hydrogen connected to the carbon C3 (positive spin density) shows a negative spin density by spin polarization mechanism which corresponds to a negative A_{iso} coupling of −14.1 MHz. The calculated values of A_{iso} for meta-hydrogens lie in a moderate range (5.1 and 7.3 MHz for H connected to C4 and C6, respectively). The estimated value of A_{iso} for freely rotating methyl protons, as computed from DFT calculations, is 24.3 MHz. This is an average value calculated from three different orientations of one of the CH_3 group protons (60°, 90°, and 120° rotation with respect to the plane of phenol ring). A more accurate computation of the A_{iso} for rotating methyl group requires a complete averaging of the calculated values of A_{iso} for all the three protons, over a series of rotational ϕ angles,[33] and will be performed in a further work. The isotropic hyperfine coupling constants for the imidazole nitrogens are very small (A_{iso} = 0.2 MHz for the amino nitrogen; A_{iso} = 0.5 MHz for the imino nitrogen) and reflect a poor spin delocalization onto the imidazole ring.

Discussion

The choice of our synthetic model for the YH structure in the heme-copper oxidases (Figure 1), 4-methyl-2-(4-methyl-imidazole-1-yl)-phenol (Figure 2), was dictated by spectroscopic considerations. The minimal model that will allow realistic interpretation of spectroscopic features that may appear in the oxidases, particularly in the infrared or Raman spectra, needs to embody structural characteristics that adequately mimic the native enzyme structures. These characteristics include the ring−ring bond at the correct position, the relevant regiochemistry, and aliphatic groups on both rings at the correct positions to mimic the amino acid side chains. As we have recently pointed out,[13] the latter are critically important for modeling the vibrational spectra, allowing us to assign IR features unique to the YH structure in the *E. coli* quinol oxidase cytochrome b_o. This view has been dramatically verified recently[34] by an infrared study of *Rhodobacter spharoides* cytochrome c oxidase, in which difference spectra reveal a YH infrared spectrum essentially identical to the one that we reported for the model 4-methyl-2-(4-methyl-imidazole-1-yl)-phenol.[34] We have recently confirmed this observation in the bovine heart cytochrome c oxidase.

The CW-EPR spectra of the 4-methyl-2-(4-methyl-imidazole-1-yl)-phenol radicals reported here are similar to those reported in a recent study.[23] This earlier study, however, was limited to a model of YH which incorporated natural abundance N-histidine. In our present work, the paramagnetic resonance spectra of the ^{15}N isotopically labeled compound ^{15}**N-5** are also reported. The CW-EPR spectrum of ^{15}**N-5** is nearly identical with that of the unlabeled **5**, demonstrating minimal hyperfine coupling of the nitrogens of the imidazole substituent. The simulations of CW-EPR spectra allow us to place the upper limit of the nitrogen couplings. However, we cannot determine the precise hyperfine values of the nitrogens of the imidazole with CW-EPR or get any information about the nuclear quadrupolar interactions for the $I = 1$ ^{14}N nitrogens. ESEEM spectroscopy of both unlabeled and ^{15}N isotopic labeled compounds demonstrate two inequivalent, weakly coupled nitrogens: one (N_A) near the "exact cancellation" condition and another (N_B) more weakly coupled. These trends are observed in the DFT calculations as well. Both our computational and experimental results, demonstrating minimal nitrogen hyperfine couplings, are consistent with density functional calculations on *o*-substituted phenols[35] and a recent EPR spectroscopy study[24] which suggest that very little change of spin density distributions on the phenol ring results from imidazole substitution.

Although specific ^{15}N labeling of the two different sites of the imidazole ring would be required to make absolutely definitive nitrogen assignments, the use of the DFT calculations to generate theoretical spectroscopic parameters can help us match the spectroscopically characterized nitrogens to the specific imino and amino nitrogens on the imidazole ring. In terms of hyperfine couplings, the DFT calculations show the larger isotropic coupling to the imino nitrogen and the smaller coupling to the amino nitrogen. Matching these calculations to the observed classes leads to an assigment of the "exact cancellation" nitrogen N_A to the imino nitrogen and the weaker coupled N_B to the amino nitrogen. We can then turn to the quadrupolar interaction to check for consistency with this assignment.

(33) Mattar, S. M.; Emwas A. H.; Stephens, A. D. *Chem. Phys. Lett.* **2002**, *363*, 152−160.

(34) Nyquist, R. M.; Heightbrink, D.; Bolwien, C.; Gennis, R. B.; Heberle, J. *Proc. Natl. Acad. Sci. U.S.A.* **2003**, *100*, 8715−8720.

(35) Himo, F.; Eriksson, L. A.; Blomberg, R. A.; Siegbahn, P. E. M. *Int. J. Quantum Chem.* **2000**, *76*, 714−723.

Table 2. NQR Parameters Calculated by DFT for **R5** Together with Experimental and Calculated Values for Similar Compounds

	amino (tricoordinate) nitrogen		imino (dicoordinate) nitrogen	
compound	C_q [MHz]	η	C_q [MHz]	η
R5 calcd	3.16	0.302	4.56	0.032
R5 expt	2.21	0.805	2.55	0.380
imidazole[a] calcd	2.64	0.133	4.08	0.067
imidazole[a] expt	2.54	0.178	4.03	0.120
N-methylimidazole[a]	2.79	0.351	4.02	0.045

[a] Reported by Torrent et al.[22]

The ESEEM-derived values of $e^2qQ = 2.50$ MHz and $\eta = 0.32$ for the N_A nitrogen in "exact cancellation" are different from the imidazole values from Nuclear Quadrupole Resonance[36] (imino ^{14}N, $e^2qQ = 3.27$ MHz and $\eta = 0.135$; amino ^{14}N, $e^2qQ = 1.44$ MHz and $\eta = 0.995$). However, assuming the nitrogen in "exact cancellation" is the imino nitrogen as suggested by the hyperfine analysis, the derived values fall on the linear anticorrelation between e^2qQ and η and attributed to the changes in 2p orbital populations on the nitrogen with the q_{zz} axis of the electric field gradient tensor located along the nitrogen lone pair orbital.[36] The parameters $e^2qQ = 2.20$ MHz, $\eta = 0.905$ assigned to the more weakly coupled nitrogen N_B are close to the values $e^2qQ = 2.198$ MHz and $\eta = 0.784$ obtained for the amino nitrogen of benzyl imidazole.[36]

Such trends are supported by DFT calculations of the quadrupolar coupling constants and asymmetry parameters for imidazole nitrogen atoms. The calculated and experimental quadrupolar coupling constants and asymmetry parameters for **R5** together with some similar molecules are listed in Table 2. The calculated values of $e^2qQ = 3.16$ MHz and $\eta = 0.302$ for the amino nitrogen and $e^2qQ = 4.56$ MHz and $\eta = 0.032$ for the imino nitrogen are in agreement with the trend observed for imidazole nitrogens, in both experimental and quantum mechanical studies:[22,36] with smaller e^2qQ values and higher asymmetry parameters η for tricoordinated amino nitrogens and larger e^2qQ values and less pronounced asymmetry (small η) for dicoordinated imino nitrogens.[37] Although the absolute values are not that similar for the calculated and ESEEM-derived couplings, both of these trends are matched by making the assignment of N_A to the imino nitrogen and N_B to the amino nitrogen of the model YH radical.

Two important comments have to be made about the calculated values of e^2qQ and η. First, it should be noticed that the values of e^2qQ in gaseous phase are usually higher by a few percent than in the solid or liquid phase, and thus our calculated e^2qQ values might be slightly overestimated. Additionally, due to the fact that the calculated values of η are drastically affected by the small changes in any of the components of the EFG tensors, the relevance of the calculated η must be only regarded in the context of established trends along a series of similar compounds.[38] Whereas, as discussed, the absolute calculated values of e^2qQ are slightly higher and η are slightly lower than the experimentally estimated ones (DFT calculated: amino nitrogen, $e^2qQ = 3.16$ MHz, $\eta = 0.302$; imino nitrogen, $e^2qQ = 4.56$ MHz, $\eta = 0.032$), they are in excellent agreement with those observed and computed for different imidazole complexes and thus these calculations support the specific imino and amino nitrogen assigments for **R5**.

We also note that the variable temperature CW spectra of the ^{15}**N-5** radical reveal a hindered rotation of the phenolic methyl group that is consistent with similar dynamical phenomena observed in CW powder spectra of $R-C^{\bullet}-CH_3$ radicals.

Conclusions

In this work, we report CW-EPR, ESEEM, and DFT calculation results of unlabeled and ^{15}N labeled model compounds relevant to the cross-linked Tyr-His of cytochrome c oxidase. The goal is to probe the hyperfine interactions with the two nitrogens of the linked imidazole as a measure of spin delocalization unto the substituent ring. CW-EPR spectra of both unlabeled and ^{15}N labeled model compounds are similar, which implies that the unpaired spin density is mostly localized on the phenol ring, with only slight delocalization onto the nitrogens of imidazole. ESEEM spectroscopy was employed to further determine the nitrogen couplings. We detect the two inequivalent imidazole ring nitrogens coupled to the phenol ring radical: the imino nitrogen is most likely the one in the exact cancellation ESEEM regime, while the amino nitrogen directly bound to the phenol ring appears most likely to be the more weakly coupled nitrogen. Altogether, the combined CW-EPR, ESEEM, and DFT work provides a coherent picture of the electronic structure of the YH model compound and confirms that the imidazole substituent has only a minor effect on the phenol radical due to a weak delocalization of the spin density to the imidazole ring. As has been demonstrated in the infrared studies,[13,34] we expected to be able to extrapolate this result to the cross-linked YH species of cytochrome c oxidase. This complementary approach using different spectroscopic techniques together with quantum mechanical calculations can be efficiently used as a valuable tool to describe the electronic structure of the model tyrosine-histidine radicals.

Acknowledgment. This work was supported by NIH Grant GM60011 and NSF Grant MCB-9874541 to R.D.B. and NIH Grant DK36263 to W.H.W.. This work was done in collaboration with the National Stable Isotope Resource (P41 RR02231), an NIH/NCRR supported research resource. The authors are grateful to professor Robert Gennis and Joachim Heberle for communication of work in press. The authors gratefully acknowledge Professor Kurt Warncke for providing the ESEEM simulation code. The work of M. Brynda was supported by Swiss National Science Foundation Grant 8220-067593.

JA0303743

(36) Ashby, C. I. H.; Cheng, C. P.; Brown, T. L. *J. Am. Chem. Soc.* **1978**, *100*, 6057−6063.

(37) For the sake of consistency, the spin density analysis and calculations of NQR and EPR couplings were also carried out on the pseudo-cis rotamer of **R5**. The spin density distribution is almost identical, and the calculated values of e^2qQ and η differ by less than 2% from the values calculated for the pseudo-trans rotamer of **R5**.

(38) Harwell, C. R.; Mrse, A. A.; Shelby, A. I.; Butler, L. G.; Hall, R. W. *J. Phys. Chem. A* **1999**, *103*, 8088−8092.